Optical trapping calculations for metal nanoparticles. Comparison with experimental data for Au and Ag spheres.

Rosalba Saija[1], Paolo Denti[1], Ferdinando Borghese[1,*], Onofrio M. Maragò[2], and Maria Antonia Iatì[2]

[1] *Dipartimento di Fisica della Materia e Ingegneria Elettronica, Università di Messina, Salita Sperone 31, 98166 Messina, Italy*

[2] *Istituto per i Processi Chimico-Fisici (Messina), Consiglio Nazionale delle Ricerche, Salita Sperone, 98158 Faro Superiore, Messina, Italy*

borghese@ortica.unime.it

Abstract: We calculate the optical forces on Au and Ag nanospheres through a procedure based on the Maxwell stress tensor. We compare the theoretical and experimental force constants obtained for gold and silver nanospheres finding good agreement for all particles with $r < 80\,\text{nm}$. The trapping of the larger particles recently demonstrated in experiments is not foreseen by our purely electromagnetic theory based on fixed dielectric properties. Since the laser power produces a heating that may be large for the largest spheres, we propose a model in which the latter particles are surrounded by a steam bubble. This model foresees the trapping of these particles and the results turn out to be in reasonable agreement with the experimental data.

OCIS codes: (290.0290) Scattering; (260.2110) Electromagnetic theory; (260.2160) Energy transfer; (140.7010) Laser trapping.

References and links

1. A. Ashkin, J. M. Dziedzic, J. E. Bjorkholm, and S. Chu S,"Observation of single-beam gradient force optical trap for dielectric particles," Opt. Lett. **11**, 288–290 (1986).
2. K. C. Neuman and S. M. Block, "Optical trapping," Rev. Sci. Instrum. **75**, 2787–2809 (2004).
3. M. Dienerowitz, M. Mazilu, and K. Dholakia, "Optical manipulation of nanoparticles: a review," J. Nanophoton. **2**, 021875 (2008).
4. L. Novotny and B. Hecht, *Principles of nano-optics*, (Cambridge University Press, Cambridge, 2006).
5. K. Svoboda and M. Block, "Optical trapping of metallic Rayleigh particles," Opt. Lett. **19**, 930–932 (1994).
6. P. M. Hansen, V. K. Bhatia, N. Harrit, and L. Oddershede, "Expanding the optical trapping range of gold nanoparticles," Nano Lett. **5**, 1937–1942 (2005).
7. L. Bosanac, T. Aabo, P. M. Bendix, and L. B. Oddershede, "Efficient optical trapping and visualization of silver nanoparticles," Nano Lett. **8**, 1486–1491 (2008).
8. Y. Seol, A. E. Carpenter, and T. Perkins, "Gold nanoparticles: enhanced optical trapping and sensitivity coupled with significant heating," Opt. Lett. **31**, 2429–2431 (2006).
9. D. Stroud, "Theory of the intensity-dependent optical activity in dilute composites," J. Appl. Phys. **66**, 2585–2588 (1989).
10. F. Borghese, P. Denti, R. Saija, and M. A. Iatì, "Optical trapping of nonspherical particles in the *T*-matrix formalism," Opt. Express **15**, 11984–11998 (2007).
11. F. Borghese, P. Denti, R. Saija, and M. A. Iatì, "Optical trapping of nonspherical particles in the *T*-matrix formalism: erratum," Opt. Express **15**, 6946 (2007).

#108098 - $15.00 USD Received 26 Feb 2009; revised 8 May 2009; accepted 3 Jun 2009; published 4 Jun 2009

12. F. Borghese, P. Denti, R. Saija, M. A. Iatì, and O. M. Maragò, "Radiation force and torque on optically trapped linear nanostructures," Phys. Rev. Lett. **100**, 163903 (2008).
13. C. Selhuber-Unkel, I. Zins, O. Schubert, C. Sönnichsen, and L. B. Oddershede, "Quantitative optical trapping of single gold nanorods," Nano Lett. **8**, 2998–3003 (2008).
14. J. D. Jackson, *Classical Electrodynamics*, 2d ed. (Wiley, New York, 1975).
15. F. Borghese, P. Denti, and R. Saija, *Scattering by model nonspherical particles*, 2d edition (Springer, Berlin, 2007).
16. F. Borghese, P. Denti, R. Saija, and M. A. Iatì, "Radiation torque on nonspherical particles in the transition matrix formalism," Opt. Express **14**, 9508–9521 (2006).
17. F. Borghese, P. Denti, R. Saija, and M. A. Iatì, " Radiation torque on nonspherical particles in the transition matrix formalism: erratum," Opt. Express **15**, 6946 (2007).
18. P. L. Marston and J. H. Crichton, "Radiation torque on a sphere caused by a circularly-polarized electromagnetic wave," Phys. Rev. A **30**, 2508–2516 (1984).
19. P. B. Johnson and R. W. Christy, "Optical constants of the noble metals," Phys. Rev. B **6**, 4370–4379 (1972).
20. A. Rohrbach, "Stiffness of optical traps: Quantitative agreement between experiment and electromagnetic theory," Phys. Rev. Lett. **95**, 168102 (2005).
21. S. N. S. Reihani, and L. B. Oddershede, "Optimizing immersion media refractive index improves optical trapping by compensating spherical aberrations," Opt. Lett. **32**, 1998–2000 (2007).
22. L. M. Liz-Marzán and P. Mulvaney, "Au@SiO_2 colloids: effect of temperature on the surface plasmons absorption," New J. Chem. **22**, 1285–1288 (1998).
23. R. H. Doremus, "Optical properties of small gold particles," J. Chem. Phys. **40**, 2389–2396 (1964).
24. R. H. Doremus, "Erratum: Optical properties of small gold particles," J. Chem Phys. **41**, 3259 (1964).
25. U. Kreibig, "Anomalous frequency and temperature dependence of the optical absorption of small gold particles," J. Phys. (Paris) **C2**, 97 (1977).
26. E. J. G. Peterman, F. Gittes, and C. F. Schmidt, "Laser-induced heating in optical traps," Biophys. J. **84**, 1308–1316 (2003).
27. D. Lapotko, "Optical excitation and detection of vapor bubbles around plasmonic nanoparticles," Opt. Express **17**, 2538–2556 (2009).
28. F. Borghese, P. Denti, R. Saija, G. Toscano, and O. I. Sindoni, "Extinction coefficient for a random dispersion of small stratified spheres and a random dispersion of their binary aggregates," J. Opt. Soc. Am. A **4**, 1984–1991 (1987).

1. Introduction

Optical tweezers [1] are a well established laboratory tool to trap and manipulate microsized and nanosized particles [2, 3]. Nevertheless, theoretical calculations are necessary for an interpretation of the experimental findings, especially in the case of nanosized metal spheres whose trapping is strongly influenced by plasmon enhancement [4]. Optical trapping of metal nanoparticles has been widely investigated experimentally since Svoboda and Block [5] stably trapped Au nanospheres. On the other hand, a careful theoretical modeling and a quantitative comparison with experiment is still lacking. Recently, a few experimental papers reported quantitative force measurements on optical trapping of Au and Ag particles [6, 7], but some of their findings are not easily explained in the framework of the customary dipole approximation [4]. Measuring the trapping force constants for metal nanoparticles is a rather hard task, although the plasmon resonances enhance the radiation force [4], because the effect of higher order plasmons increases when larger and larger particles are considered. Moreover, optical trapping of dielectric particles requires a few milliwatts of laser power whereas metal particles may require higher powers of the order of 100 milliwatts and more [6, 7, 8]. Using such a comparatively large power may bias the measurements of the force constants, because of the consequent heating both of the particles and of the surrounding medium [8] and possibly because of the change of the relative refractive index of the particles due to the large field intensity [9].

In the present paper we calculate the optical forces on gold and silver nanospheres with the purpose of checking up to what size our theoretical approach foresees the trapping of spherical particles of the noble metals mentioned above. For our investigation we exploit the theory that we recently developed and successfully applied to the calculation of the optical forces on dielectric spheres [10, 11] as well as of the torques exerted on model elongated dielectric

#108098 - $15.00 USD Received 26 Feb 2009; revised 8 May 2009; accepted 3 Jun 2009; published 4 Jun 2009

nanostructures [12]. In principle, our theory could be applied also to elongated metallic nanostructures such as those trapped by Selhuber-Unkel et al. [13]. However, we defer this task for future work because also the interpretation of the experiments for much simpler systems, such as spherical metallic particles, presents a hunk of problems that will become evident later. Our theory is based on the expansion of the field in a series of vector multipole fields and on the imposition of the customary boundary conditions across the surface of the particles. Then, we do not resort to the typical separation of the optical force into a gradient and a scattering contribution, but make full use of the formalism based on the Maxwell stress tensor, in the form of Minkowski, as given, e.g., by Jackson [14]. This approach does not require the particles to be small or homogeneous whereas the customary separation into scattering and gradient force requires the particles to be small with respect to the wavelength and that their absorptivity be small [4].

The paper is organized as follows: in Sec. 2 we give a sketch of the main formulas on which the calculations are based (see also [10, 11] for more details), in order to give a better insight into our results on metal nanoparticles, that are fully discussed in Sec. 3.

2. Sketch of the theory

The geometry that we adopt to calculate the radiation force exerted by a focalized laser beam on a particle is sketched in Fig. 1. The center of mass of the particle is located at $\mathbf{R}_{O'}$ with respect to a cartesian frame of reference whose origin O coincides with the nominal focus F of the lens and whose z axis marks the direction of propagation of the beam. The radiation force can be written as [14]

$$\mathbf{F}_{\mathrm{Rad}} = r'^2 \int_{\Omega'} \hat{\mathbf{r}}' \cdot \langle \mathsf{T}_{\mathrm{M}} \rangle \, \mathrm{d}\Omega' \,, \tag{1}$$

where r' is the radius of a large spherical surface surrounding the particle and T_{M} is the time averaged Maxwell stress tensor

$$\mathsf{T}_{\mathrm{M}} = \frac{1}{8\pi}\left[n^2 \mathbf{E}' \otimes \mathbf{E}'^{*} + \mathbf{B}' \otimes \mathbf{B}'^{*} - \frac{1}{2}\left(n^2 \mathbf{E}' \cdot \mathbf{E}'^{*} + \mathbf{B}' \cdot \mathbf{B}'^{*}\right)\mathsf{I}\right] .$$

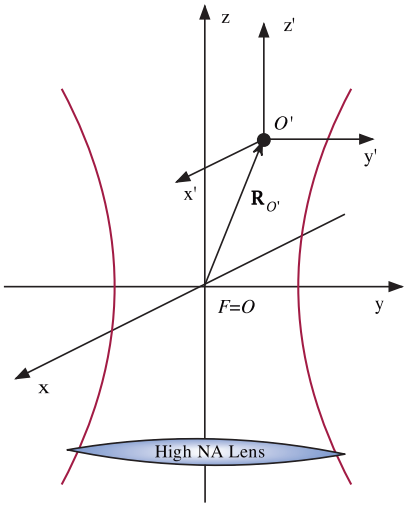

Fig. 1. Sketch of the trapping geometry. The particle is located at $\mathbf{R}_{O'}$ with respect to a cartesian frame of reference whose origin O coincides with the nominal focus F of the lens.

#108098 - $15.00 USD Received 26 Feb 2009; revised 8 May 2009; accepted 3 Jun 2009; published 4 Jun 2009

In the definition above n is the refractive index of the medium that embeds the particle, $\otimes$ denotes dyadic product, and I is the unit dyadic. The fields $\mathbf{E}'$ and $\mathbf{B}'$ are considered in a frame of reference with origin at $\mathbf{R}_{O'}$ and are the superposition of the incident radiation field and of the field scattered by the particle.

We start by considering the incident field to be a simple plane wave of amplitude E_0' and (circular) frequency ω, and by expanding all the fields in a series of spherical vector multipole fields we are able to write the component of the radiation force along a direction characterized by the unit vector $\hat{\mathbf{v}}_\zeta$ as

$$F_{\mathrm{Rad}\,\zeta} = -F^{(\mathrm{Sca})}_{\mathrm{Rad}\,\zeta} + F^{(\mathrm{Ext})}_{\mathrm{Rad}\,\zeta}\,, \tag{2}$$

where

$$F^{(\mathrm{Sca})}_{\mathrm{Rad}\,\zeta} = \frac{2|E_0'|^2}{16\pi k_\mathrm{v}^2}\mathrm{Re}\sum_{plm}\sum_{p'l'm'} A^{(p)*}_{lm} A^{(p')}_{l'm'} i^{l-l'} I^{(pp')}_{\zeta\, lml'm'}\,, \tag{3a}$$

$$F^{(\mathrm{Ext})}_{\mathrm{Rad}\,\zeta} = -\frac{2|E_0'|^2}{16\pi k_\mathrm{v}^2}\mathrm{Re}\sum_{plm}\sum_{p'l'm'} W^{(p)*}_{\mathrm{I}lm} A^{(p')}_{l'm'} i^{l-l'} I^{(pp')}_{\zeta\, lml'm'}\,. \tag{3b}$$

In Eqs. (3) the multipole amplitudes of the incident field $W^{(p)*}_{\mathrm{I}lm}$ are known [10], and those of the scattered field $A^{(p)}_{lm}$ can be calculated, e.g., by solving the linear system of equations that describes the boundary conditions [15]. The quantities $I^{(pp')}_{\zeta\, lml'm'}$ are integrals that can be calculated in closed form [10, 11]. $k_\mathrm{v} = \omega/c$, where c is the speed of light.

Even in our approach the radiation force has been separated into two contributions, but there is no similarity with the customary separation into a field gradient contribution and a scattering contribution. The separation effected in Eqs. (3a) and (3b) can be tracked back to Eq. (1) which, due to the structure of the Maxwell stress tensor, includes $|\mathbf{E}'_\mathrm{S}|^2$ and $\mathbf{E}'^*_\mathrm{I}\cdot\mathbf{E}'_\mathrm{S}$ as well as the corresponding terms from the magnetic field. When these terms are expanded as a series of multipole fields we just get $F^{(\mathrm{Sca})}_{\mathrm{Rad}\,\zeta}$, that depends on the multipole amplitudes of the scattered field, and $F^{(\mathrm{Ext})}_{\mathrm{Rad}\,\zeta}$ that depends on the multipole amplitudes both of the incident and of the scattered fields. As a result, $F^{(\mathrm{Sca})}_{\mathrm{Rad}\,\zeta}$ and $F^{(\mathrm{Ext})}_{\mathrm{Rad}\,\zeta}$ can be somehow related to the scattering and to the extinction cross section of the particle, respectively, and the radiation force can loosely be related to the absorption cross section, i.e., to the absorptivity of the particle. Note that similar considerations hold true also for the radiation torque [16, 17]: in particular for a spherical scatterer the torque exerted by an elliptically polarized plane wave can be explicitly written in terms of the difference of the extinction and of the scattering cross section [18].

Now, let the incident field be not a single plane wave but a focused laser beam. Equations (3a) and (3b) still apply provided the following substitutions are introduced [10]

$$E_0' W^{(p)}_{\mathrm{I}lm} \to \mathscr{W}^{(p)}_{lm}(\mathbf{R}_{O'})\,, \quad E_0' A^{(p)}_{lm} \to \mathscr{A}^{(p)}_{lm}\,,$$

where the quantities $\mathscr{W}^{(p)}_{lm}(\mathbf{R}_{O'})$ are the amplitudes of the incident laser field and $\mathscr{A}^{(p)}_{lm}$ are the corresponding amplitudes of the scattered field. The explicit formulas for the calculation of these amplitudes are reported in [10]. Instead here we want to remark some features of our approach that are crucial for the discussion on metal particles in Sec. 3.

- First, Eqs. (3a) and (3b) do not require the particles to be small or homogeneous. Large particles, even of high absorptivity, can be dealt with by these equations. The case of radially inhomogeneous spheres, e.g., layered spheres, can also be dealt without any difficulty.

#108098 - $15.00 USD Received 26 Feb 2009; revised 8 May 2009; accepted 3 Jun 2009; published 4 Jun 2009

- Second, we shall see later that the relative magnitude of the contributions of Eqs. (3a) and (3b) depends on the radius of the particles and plays a fundamental role in determining the trapping.
- Third, the force calculated through Eqs. (3a) and (3b) is a linear function of the laser power, as is expected from any purely electromagnetic theory of the trapping forces. However, when interpreting the results of any experiment, one should consider that using a large electromagnetic power may alter the parameters of the model, such as, e.g., the refractive index or the very geometry of the particles subject to the force.

3. Results and discussion

A critical point in the calculation of the radiation force, whatever the approach one chooses to use, is the knowledge of the dielectric properties of the particles. In the present paper we compare our calculations with the experimental findings of Hansen et al. [6] and of Bosanac et al. [7], that were obtained at $\lambda = 1064$ nm. Therefore, we chose, both for Au and Ag nanospheres, the dielectric function tabulated by Johnson and Christy [19], whose use leads to a good agreement between calculated and experimental extinction spectra of such nanoparticles. In Fig. 2 we report these calculated extinction cross sections of Au and Ag nanospheres of various sizes. The main feature of both metals is the structure of the plasmon resonances whose position and complexity depends on the radius of the particles. We also notice that at $\lambda = 1064\,\mathrm{nm}$ both Au particles with $r = 77\,\mathrm{nm}$ and Ag particles with $r = 80\,\mathrm{nm}$ still show a large extinction in comparison with particles of smaller radius.

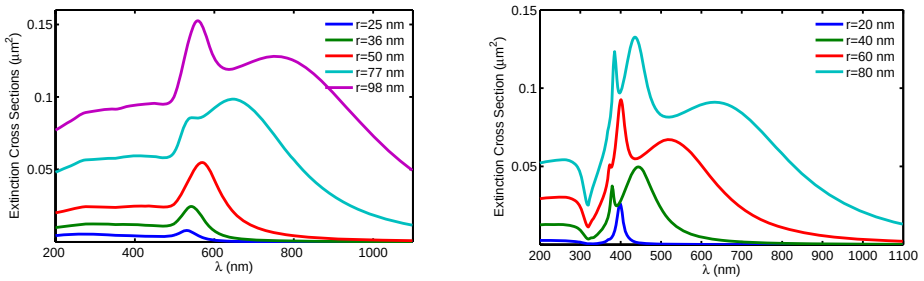

Fig. 2. Extinction cross section of Au (left) and Ag (right) spheres. The refractive index is the one tabulated by Johnson and Christy [19].

The other parameters that we adopt in our calculations are those of Hansen et al. for Au particles and of Bosanac et al. for Ag particles. Thus, we assume an optical system with numerical aperture NA=1.2 in water illuminated by a x-polarized TEM_{00} laser beam. Since both in [6] and [7] the objective has been only slightly overfilled, we chose the filling factor $f_0 = 2$ according to the common choice reported in the literature [4, 10, 20]. We also consider the case of an oil immersion lens, and consequently change the numerical aperture to NA=1.32. However, we did not compensate for the spherical aberration by using oils of different refractive indexes [21]. In fact, we use $n_{\mathrm{oil}} = 1.54$ and consider several values of d_{w}, the distance from the nominal focus of the cover slip that separates oil from water, as in all cases the particles are embedded in water. According to Hansen et al. [6], the effect of the aberration produced by the presence of the cover slip can be minimized by locating the latter as near as possible to the trapping volume. On the other hand, in [6] it is stressed that the effect of the aberration is to reduce the maximum size of the trappable particles and that the best results are obtained using a water immersion lens. Since trapping particles of different size require different powers of the laser beam, in [6, 7] the

#108098 - $15.00 USD Received 26 Feb 2009; revised 8 May 2009; accepted 3 Jun 2009; published 4 Jun 2009

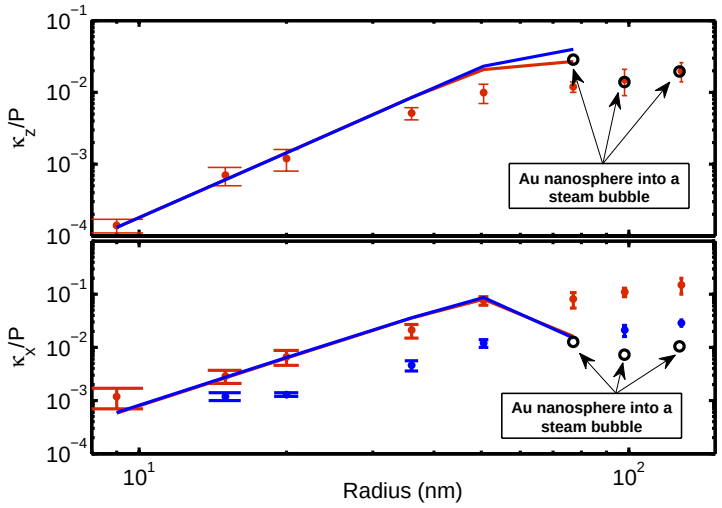

Fig. 3. Experimental (from [6]) and calculated stiffness κ_z/P and κ_x/P in $\mathrm{pN}/(\mathrm{nm}\cdot\mathrm{W})$ for gold spheres, both for water immersion (red line and points) and for oil immersion lens (blue lines and points). The points marked by an arrow refer to particles embedded into a steam bubble.

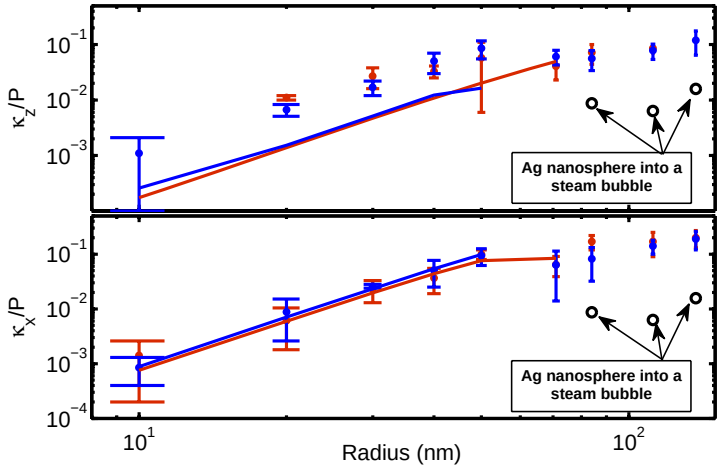

Fig. 4. Experimental (from [7]) and calculated stiffness κ_z/P and κ_x/P in $\mathrm{pN}/(\mathrm{nm}\cdot\mathrm{W})$ for silver spheres, both for water immersion (red lines and points) and for oil immersion lens (blue lines and points). The points marked by an arrow refer to particles embedded into a steam bubble.

experimental stiffnesses of the trap are normalized to the laser power P. Our calculated κ_z/P and κ_x/P vs. the size of the spheres for Au particles are reported in Fig. 3 together with the experimental data of Hansen et al. [6], whereas the results for Ag spheres are reported in Fig. 4 together with the experimental findings of Bosanac et al. [7]. Figures 3 and 4 also include some points that are marked by an arrow: these points will be discussed later. At present, we see at once that we do not succeed in the trapping of spheres with $r > 77\,\mathrm{nm}$, whereas Hansen

#108098 - $15.00 USD Received 26 Feb 2009; revised 8 May 2009; accepted 3 Jun 2009; published 4 Jun 2009

et al. and Bosanac et al. were able to trap Au spheres with r up to 127 nm and Ag spheres with r up to 137.5 nm, respectively. Nevertheless, in [6] the authors stress that they were unable to get stable trapping of Au spheres with $r = 77$ nm, whereas Bosanac et al. [7] notice that their measured stiffnesses for Ag spheres with $r = 80$ nm are much lower than expected. In a sense, this is not surprising, because the experimental measurements include all effects, linear and nonlinear, yielded by the radiation field with scarce or no possibility of discrimination. On the other hand, our calculations are performed for fixed parameters of the model, i.e., fixed radius and refractive index of the particles, and fixed refractive index of the surrounding medium.

Hansen et al. report their measured κ_z/P for the nonaberrated setup only, but our calculated curves for nonaberrated and aberrated setup, provided $-6\,\mu\text{m} \leq d_\text{w} \leq -2\,\mu\text{m}$, are almost indistinguishable from each other and show a good agreement with the experimental data up to radii at which trapping is predicted by the theory. A good agreement is also attained in Fig. 4 for κ_z/P of Ag, although our results are an order of magnitude lower than the experimental data. Our results for κ_x/P in Figs. 3 and 4 show that the calculated curves for nonaberrated and aberrated setup are quite superposable, and agree rather well with the experimental data for the nonaberrated setup. In fact, the experimental data of Au for aberrated and nonaberrated setup show strong differences. We believe that this is due to experimental difficulties in the power normalization when using oil immersion objectives. At the same time, we note that the experimental κ_x/P for Ag particles show a negligible dependence on the setup, because of the optimization criterion of Reihani et al. [21].

In Figs. 3 and 4 a clear size scaling is evident for small radii. The optical trapping stiffnesses lie on mutually parallel lines with slope 3 on a log-log scale, thus showing the existence of a scaling law with the volume of the particle. The fact that our calculated results change their slope for radii larger that 50 nm suggests the transition from a proportionality to the volume to a dependence on some other feature. Indeed, in the range of radii between 70 and 80 nm there occur a change in the trapping regime. In order to understand the mechanism of this change we first studied the behavior of the radiation force for different values of d_w, i.e., when aberration can play a significant role in degrading the trapping in the axial direction. We report the results of our study in graphical form for Au spheres only, since the results for Ag spheres are quite similar. Thus, in Fig. 5 (left) we report the z component of the trapping efficiency Q_z for Au spheres with $r = 25$ nm. Let us recall that the definition of Q_z is

$$Q_z = F_{\text{Rad}\,z}\frac{c}{nP}\,.$$

The trapping occurs when the trapping efficiency vanishes with a negative derivative, and according to Fig. 5 (left) this occurs for aberrated ($d_\text{w} \neq 0$) and nonaberrated ($d_\text{w} = 0$) configuration. In particular, the trapping occurs almost at the nominal focus for nonaberrated configuration with the largest value of the stiffness κ_z. When we go to consider spheres with $r = 77$ nm, Fig. 5 (right), we see at once that the trapping is almost nonoccurring for the aberrated configurations whereas it only occurs, but weakly, for the nonaberrated configuration. This is in agreement with the claim of Hansen et al. [6] that the best results are obtained using a water immersion objective.

Further insight into the trapping mechanism can be gained by considering the relative importance of the contributions to the radiation force from $F^{(\text{Ext})}_{\text{Rad}\,z}$, Eq. (3b), and $F^{(\text{Sca})}_{\text{Rad}\,z}$, Eq. (3a). In Fig. 6 we report $F^{(\text{Ext})}_{\text{Rad}\,z}$ (left) and $F^{(\text{Sca})}_{\text{Rad}\,z}$ (right), calculated per unit incident power, as a function of z on Au spheres for several values of their radius. By following the evolution of these two contributions as a function of the radius, we see that $F^{(\text{Sca})}_{\text{Rad}\,z}$ does not vanish but is at least 2 orders of magnitude smaller than $F^{(\text{Ext})}_{\text{Rad}\,z}$ up to $r = 50$ nm. As a consequence the trapping position is mainly determined by the vanishing of $F^{(\text{Ext})}_{\text{Rad}\,z}$ with a negative derivative. This is most

#108098 - $15.00 USD Received 26 Feb 2009; revised 8 May 2009; accepted 3 Jun 2009; published 4 Jun 2009

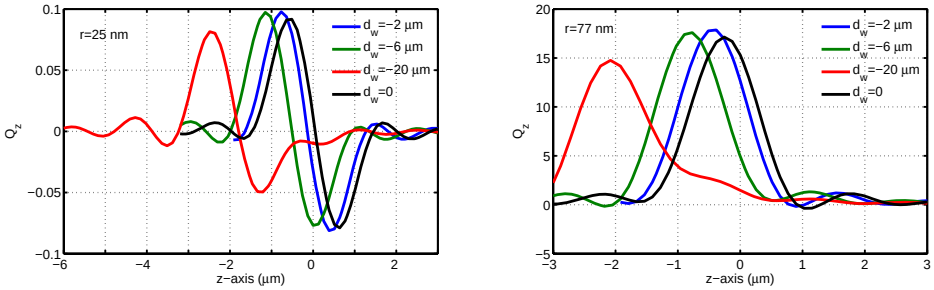

Fig. 5. Trapping efficiency for Au spheres with $r = 25\,\mathrm{nm}$ (left) and $r = 77\,\mathrm{nm}$ (right) at $\lambda = 1064\,\mathrm{nm}$. The nominal focus of the lens is at $z = 0$. $d_\mathrm{w} \neq 0$ denotes the position of the cover slip for the case of oil immersion objective, and the curve for $d_\mathrm{w} = -2\,\mu\mathrm{m}$ is truncated at the position of the cover slip.

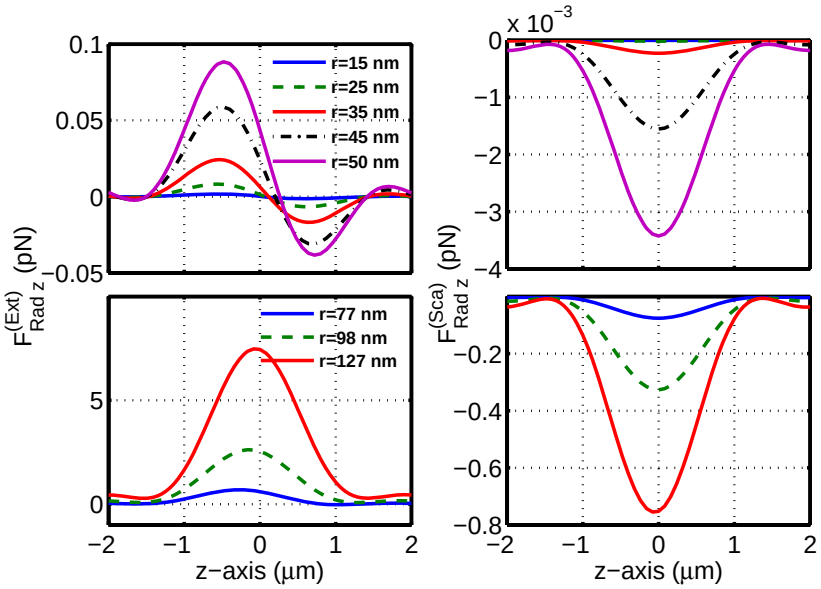

Fig. 6. $F^{(\mathrm{Ext})}_{\mathrm{Rad}z}$ (left) and $F^{(\mathrm{Sca})}_{\mathrm{Rad}z}$ (right) as a function of z for Au spheres of small (top) and large (bottom) radius

easily seen in Table 1 in which we report, for each radius, both for Au and for Ag, the actual trapping position and the one that would be determined by the vanishing of $F^{(\mathrm{Ext})}_{\mathrm{Rad}z}$ alone, i.e., by putting $F^{(\mathrm{Sca})}_{\mathrm{Rad}z} \equiv 0$. On the contrary, $F^{(\mathrm{Ext})}_{\mathrm{Rad}z}$ for $r > 77\,\mathrm{nm}$ becomes everywhere nonvanishing. Moreover, $F^{(\mathrm{Sca})}_{\mathrm{Rad}z}$ beyond being negative, becomes comparable to $F^{(\mathrm{Ext})}_{\mathrm{Rad}z}$. Thus, when $F^{(\mathrm{Sca})}_{\mathrm{Rad}z}$ is *subtracted* from $F^{(\mathrm{Ext})}_{\mathrm{Rad}z}$ to get the total optical force according to Eq. (2), one easily sees that it does not help to get the trapping. The combined behavior of $F^{(\mathrm{Ext})}_{\mathrm{Rad}z}$ and $F^{(\mathrm{Sca})}_{\mathrm{Rad}z}$ also explains the borderline weak trapping of the $r = 77\,\mathrm{nm}$ spheres.

The behavior of the radiation force in the region in which the trapping of spheres with $r > 80\,\mathrm{nm}$ might occur, strongly suggests that a given model with parameters chosen once for all cannot explain the trapping of the larger particles: the theory is linear in the power, indeed. We

#108098 - $15.00 USD Received 26 Feb 2009; revised 8 May 2009; accepted 3 Jun 2009; published 4 Jun 2009

Table 1. Trapping positions of Au and Ag nanospheres. r is the radius of the spheres used in [6, 7], z_T is the calculated trapping position, and z_E the trapping position determined by the extinction contribution alone. r, z_T, and z_E are all in nm.

Au			Ag		
r	z_T	z_E	r	z_T	z_E
15	40	40	20	16	16
25	65	64	30	47	45
35	118	113	40	116	107
45	213	200	50	234	213
50	283	262	71	708	632
77	916	841	-	-	-

must thus consider the possibility that the parameters of the model, essentially the refractive index, may change with increasing power. In this respect, it is quite natural to suspect the heating both of the medium and of the particles due to the use of a large laser power. Therefore, we first considered the study of Liz-Marzán and Mulvaney [22] who measured the change of the dielectric properties of Au colloids, more precisely of the surface plasmon absorption, in the temperature range 14–70° C. These authors, after carefully considering all the physical effects that stem from the increase of temperature, were led to the conclusion that the most important factor is the change of resistivity of gold with a consequent change of its refractive index. Nevertheless, the experiments of Liz-Marzán and Mulvaney [22] were performed on Au spheres with an average diameter $d = 15\,\text{nm}$. When the corrections that they suggest on the basis of the findings of Doremus [23] and of Kreibig [25] (these corrections depend on the size of the particles) are calculated for spheres with a radius $r \geq 77\,\text{nm}$, the change of the refractive index turns out to be negligible and leads to no increase of the radius of the trappable particles.

Next, we considered that, according to Hansen et al., the power needed to trap the larger Au spheres was of 135 mW, and that Seol et al. [8] in their study of the heat developed by the trapping beam, estimate an increase of temperature at the surface of Au nanospheres as high as $260^\circ\,\text{C/W}$. Much lower temperatures were estimated by Peterman et al. [26] at the surface of dielectric particles, but in a recent paper Lapotko [27] demonstrated that the laser-induced heating around plasmonic nanoparticles, in particular Au nanospheres, may excite detectable vapor bubbles. These studies suggested us to use the formulas reported by Seol et al. [8] to estimate the change of temperature, with respect to room temperature, at 5 nm from the surface of the Au and Ag nanospheres considered in [6] and [7]. The results of our estimate are reported in Table 2 where we also reported the absorption cross sections that, unlike [8], we calculated without resorting to the dipole approximation. The other parameters were taken as reported by Seol et al. because they are compatible even with our focalized beam.

The increases of temperature reported in Table 2 should be taken with some caution as they are due to a simplified model of the thermal equilibrium of the naked metal spheres and the surrounding water, yielding perhaps too large values for the largest Au spheres. Anyway, these increases turn out to be large enough to justify the working hypothesis that the particles, especially the largest ones, may become embedded into a steam bubble. In turn, the presence of a steam bubble, provided it is stable enough, will attenuate the effect of the metallic nature of the particles. Of course, we kept the thickness of the steam layer, which we assumed to have the refractive index $n_{\text{steam}} = 1$, as small as possible, just for the sake of stability, and made also the assumption that the particle remains steadily at the center of the bubble. Thus we calculated the

#108098 - $15.00 USD Received 26 Feb 2009; revised 8 May 2009; accepted 3 Jun 2009; published 4 Jun 2009

Table 2. Temperature change with respect to room temperature for the Au and Ag nanospheres used in [6] and [7] at their trapping position. r is the radius (in nm) of the spheres used in [6, 7], σ_{abs} (in μm^2) is the absorption cross section, and $\Delta T/P$ is the change of temperature (in K/W) due to heating by the trapping beam. ΔT has been estimated using the formulas in [8] at 5 nm from the surface of the nanospheres.

Au			Ag		
r	σ_{abs}	$\Delta T/P$	r	σ_{abs}	$\Delta T/P$
15	3.48×10^{-6}	36.43	20	1.02×10^{-6}	8.53
25	1.87×10^{-5}	130.46	30	4.14×10^{-6}	24.72
35	6.01×10^{-5}	313.75	40	1.15×10^{-5}	53.55
45	1.47×10^{-5}	614.78	50	2.57×10^{-5}	97.73
50	2.15×10^{-4}	817.74	71	9.21×10^{-5}	253.09
77	1.05×10^{-3}	1679.90	84	2.54×10^{-4}	597.55
98	2.50×10^{-3}	5072.50	112	4.31×10^{-4}	769.23
127	4.61×10^{-3}	7303.20	137	6.09×10^{-4}	896.24

field scattered by the stratified particle that includes the metal nanosphere surrounded by the steam layer and embedded into water. This has been done by exploiting the procedure that we developed just to study the resonances of layered metal spheres [28]. The resulting scattered field, when introduced into the Maxwell stress tensor, yields through Eq. (1) the radiation force acting on the center of mass of the particle. Our results for $F^{(Ext)}_{Rad\,z}$ and $F^{(Sca)}_{Rad\,z}$ on Au spheres are summarized in Fig. 7. The spheres with $r = 98$ nm are surrounded by a steam bubble with thickness 100 nm, and those with $r = 127$ nm are surrounded by a bubble with thickness 130 nm. We stress that the total diameters (particle plus bubble) are smaller than the width of the trapping spot and of the resolution of the imaging system used in the experiments. We also included the results for spheres with $r = 77$ nm surrounded by a steam layer with thickness 5 nm in order to see whether the presence of the bubble improves the trapping. All the calculations were per-

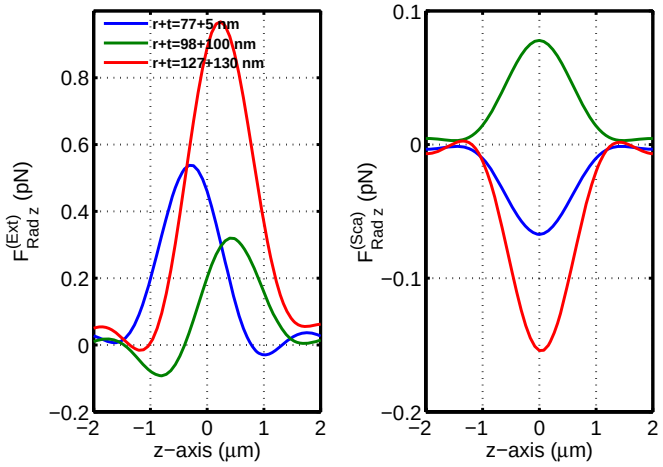

Fig. 7. $F^{(Ext)}_{Rad\,z}$ (left) and $F^{(Sca)}_{Rad\,z}$ (right) as a function of z for Au spheres in a steam bubble.

#108098 - $15.00 USD Received 26 Feb 2009; revised 8 May 2009; accepted 3 Jun 2009; published 4 Jun 2009

formed in the absence of aberration. By comparing the lower panels of Fig. 6 with Fig. 7 we

Table 3. Trapping positions of Au and Ag nanospheres embedded into a steam bubble. r is the radius of the spheres used in [6, 7], t the thickness of the steam layer, z_T is the calculated trapping position, and z_E the trapping position determined by the extinction contribution alone. r, t, z_T, and z_E are all in nm.

Au			Ag		
$r+t$	z_T	z_E	$r+t$	z_T	z_E
77+5	864	781	84+10	880	752
98+100	-1492	-1470	112+130	-1430	-1444
127+130	-1379	-1362	137+160	-1382	-

see that the extinction contribution or the $r = 77$ nm spheres into a bubble still vanishes with a negative derivative at about the same z at which it vanishes for the bare sphere. At this value of z the scattering contribution is small and, although negative, when subtracted from the extinction contribution is not able to destabilize the trapping. The new results come for the $r = 98$ nm and the $r = 127$ nm spheres whose extinction contribution alone would grant the trapping for a negative value of z. The scattering contribution, being slightly positive at the trapping position, would increase the stability for the 98 nm spheres. Also the scattering contribution for the 127 nm spheres is positive at the trapping point so that we find again an increase of stability. Although we do not report specific figures, similar results were found for the Ag spheres. We report in Table 3 all the trapping positions both for gold and silver spheres, together with the thickness of the steam layer. However, we stress that the trapping of the $r = 137$ nm Ag spheres is granted only by surrounding them with a steam bubble with a thickness as large as 160 nm, i.e., noticeably larger than the radius of the spheres, and that the extinction contribution alone is not able to produce trapping. We have no explanation for this difference but we notice that the specific heat of Ag is about two times the value for gold; a further analysis of this point is beyond the purpose of the present investigation.

The stiffnesses of the trap for spheres into a steam bubble are reported and marked by arrows in Fig. 3 for Au and in Fig. 4 for Ag. We see at once that our calculated values of κ_z/P for gold, rather surprisingly, coincide with the experimental values. In particular the addition of the bubble to the 77 nm spheres produces little change of κ_z/P. As for κ_x/P, we see that for 77 nm spheres it lies on the calculated curve, whereas, for the largest spheres, it lies on a line parallel to the experimental data. As regards Ag spheres we see that the calculated stiffnesses in the presence of a steam bubble are rather lower than the experimental data. In a sense this confirms the finding of Bosanac et al. that the experimental stiffnesses for these spheres turn out to be lower than expected.

We conclude the present investigation by remarking that an electromagnetic theory that goes beyond the dipole approximation is able to give a reliable quantitative interpretation of the experimental data on trapping of Au and Ag nanospheres. Nevertheless, when large laser powers need to be used, one should in principle consider also effects that may change the dielectric properties of the particles and of their near environment. Furthermore, a detailed investigation of the heat flow is necessary in order to formulate a physically reliable model for the optical trapping of metal particles in a focused beam of high intensity. On the other hand, although our oversimplified model of particles into a steam bubble should be considered as a working hypothesis, it definitely gives an acceptable agreement with the available experimental data.

#108098 - $15.00 USD Received 26 Feb 2009; revised 8 May 2009; accepted 3 Jun 2009; published 4 Jun 2009